energies

MDPI

Article

Synthesis of the Current Controller of the Vector Control System for Asynchronous Traction Drive of Electric Locomotives

Sergey Goolak [1], Viktor Tkachenko [1], Svitlana Sapronova [2], Vaidas Lukoševičius [3,*], Robertas Keršys [3], Rolandas Makaras [3], Artūras Keršys [3] and Borys Liubarskyi [4]

[1] Department of Electromechanics and Rolling Stock of Railways, State University of Infrastructure and Technologies, Kyrylivska Str., 9, 04071 Kyiv, Ukraine; gulak_so@gsuite.duit.edu.ua (S.G.); v.p.tkachenko@gsuite.duit.edu.ua (V.T.)
[2] Department of Cars and Carriage Facilities, State University of Infrastructure and Technologies, Kyrylivska Str., 9, 04071 Kyiv, Ukraine; sapronova_sy@gsuite.duit.edu.ua
[3] Faculty of Mechanical Engineering and Design, Kaunas University of Technology, Studentų Str., 56, 51424 Kaunas, Lithuania; robertas.kersys@ktu.lt (R.K.); rolandas.makaras@ktu.lt (R.M.); arturas.kersys@ktu.lt (A.K.)
[4] Department of Electrical Transport and Diesel Locomotive, National Technical University "Kharkiv Polytechnic Institute", Kyrpychova Str., 2, 61002 Kharkiv, Ukraine; borys.liubarskyi@khpi.edu.ua
* Correspondence: vaidas.lukosevicius@ktu.lt

Abstract: This paper deals with the analysis of the operating conditions of traction drives of the electric locomotives with asynchronous traction motors. The process of change of the catenary system voltage was found to have a stochastic character. The method of current controller synthesis based on the Wiener–Hopf equation was proposed to enable efficient performance of the traction drive control system under the condition of the stochastic nature of the catenary system voltage and the presence of interferences, when measuring the stator current values of the tractor motor. Performance simulation of the proposed current controller and the current controller used in the existing vector control systems of the traction drives used in the electric locomotives was implemented. The results of the performance simulation of the proposed current controller were compared with the performance of the current controller in existing vector control systems of the traction drives. The results are applicable to the design of vector control systems of traction drives in electric locomotives and to the study of the influence of performance of electric traction drives in electric locomotives on the quality indicators of the power supplied by the traction power supply system under the actual operating conditions of the locomotive.

Keywords: optimal controller; traction drive; vector control system

Citation: Goolak, S.; Tkachenko, V.; Sapronova, S.; Lukoševičius, V.; Keršys, R.; Makaras, R.; Keršys, A.; Liubarskyi, B. Synthesis of the Current Controller of the Vector Control System for Asynchronous Traction Drive of Electric Locomotives. *Energies* **2022**, *15*, 2374. https://doi.org/10.3390/en15072374

Academic Editors: Larysa Neduzha, Jan Kalivoda and Abu-Siada Ahmed

Received: 23 February 2022
Accepted: 22 March 2022
Published: 24 March 2022

1. Introduction

The selection of an optimal control option for specific technical applications should be based on the reasonably selected methods appropriate for the respective objects. In terms of traction drive control in an AC electric locomotive, the choice should account for a series of potential uncertainties. These uncertainties are primarily related to the operating conditions of AC electric locomotives. Studies [1–3] have shown that the voltage change process in the catenary system of the AC traction power supply network is a stochastic process. The stochastic character of the voltage change process in the catenary system of the traction power supply network is determined by the conditions under which the electric rolling stock passes through the feeder zone [4,5], the electromagnetic compatibility of the units of the electric rolling stock that are located in a single feeder zone at the quality of same time [3,6], and the current collection quality [7–9].

It should also be noted that the load of the traction drive in an electric rolling stock changes as the wheel of the electric rolling stock interacts with the rail. Several studies have been dedicated to this problem. The study [10] investigates the influence of curved line track spans on the traction drive load. The influence of the track profile on the characteristics of the traction drive has been demonstrated in studies [11,12]. The investigation of the wheel-rail friction coefficient can be found in the study [13]. An analysis of studies dedicated to the interaction of the influence of the electric rolling stock (ERS) wheel on the characteristics of the traction drive has suggested that the change in load of the electric rolling stock traction drive also has a stochastic character. In summary, an analysis conducted on the influence of the operating conditions of the ERS on the electromechanical processes in the traction drive has suggested the following conclusion: both the change of voltage in the catenary system and the change of the traction drive load have a stochastic character. The stochastic character of the variation in the voltage of the catenary system and the moment of load of the traction drive leads to greater losses in the traction motors [14] and affects the stability of performance of the traction drive control system [15–17].

In view of the stochastic character of variation of the voltage parameters of the catenary network and the traction drive load, it would be particularly practical to analyze the electromechanical processes in the traction drive system under the actual operating conditions of the AC electric locomotives. Practicality is primarily related to the fact that the above factors act on the quality of drive control. The quality of drive control, in turn, is associated with losses in the drive, which act on the energy efficiency of the performance of the traction drive system. The control system is responsible for the quality of control in the traction drive system. An analysis of traction drive systems in AC electric locomotives has suggested that asynchronous motors are the most widely used traction motors in contemporary AC electric locomotives [18]. Study [18] also provides the topologies for the design of traction drive control systems using the asynchronous motor. The control systems for this kind of drive may be the following: scalar, vector, and direct torque control (DTC).

The scalar control system belongs to the category of design-free open-loop control systems [19,20]. Open-loop control systems do not offer any possibilities for optimization of the control algorithm. Optimal control systems are designed on the basis of closed-loop control systems [21–23].

DTC systems [24–26] and vector control systems [27–29] belong to the category of design-closed-loop automatic control systems. This category of systems offers the possibility to apply the principles of optimal control [21–23].

The vector control systems of traction drives have become the most widespread systems in rolling stocks [18]. As a result, a major focus is placed on vector control systems. Comparison of the strengths and drawbacks of vector control systems versus DTC [27–29] has suggested that, in contrast to DTC systems, the drawbacks of vector control systems may include slow response to change in the resistance torque of the traction drive. In light of this drawback of vector control systems, the stochastic character of the change in the traction drive load can be further ignored. Hence, optimization of performance of the vector control system should account for the stochastic character of only the process of change of voltage in the catenary system.

Two directions can be identified in the design of the optimal control systems: optimization of performance of the overall system, and optimization of individual elements of the system, i.e., the controllers. Traction drive control systems are designed on the basis of the energy efficiency criterion [30,31].

In terms of energy efficiency, the Pontryagin criterion is the most effective when designing optimal control systems [32,33]. However, the design of the control system that is optimal by Pontryagin's criterion has certain implications. The implications stem from the double-channel character of the vector system. Here, the control is implemented using two channels: flux linkage channel and speed channel. It should also be noted that the control using the two channels is distributed by time: the flux linkage control channel is the first to operate, and the speed channel is activated after the former has completed

its operation [27–29]. This entails certain difficulties in the practical implementation of this kind of system [34].

This issue can be solved by analytic design of optimal controllers. Proportional integral controllers (PI) are used as current controllers in electric locomotives with vector control systems. The parameters of this kind of controller are based on the design of the desired logarithmic amplitude-frequency characteristic of the current control circuit [27–29]. This approach can be considered appropriate in view of the hypothesis that the process of change of the stator currents in an asynchronous motor is deterministic. As demonstrated above, this process is stochastic under the actual operating conditions of electric locomotives. Furthermore, another factor that influences the quality of control has not been taken into account in the design of this kind of controllers in these systems [27–29]. It is related to the following circumstances. In a vector control system, current sensors are activated in the feedback of the current control channel. Sensors enable identification of the present values of the phase currents of the asynchronous motor stator. Electromagnetic interference of the current sensors is caused by the asynchronous traction motor. These interferences are usually so-called 'white noise', that is, they have zero mathematical expectation and nonzero dispersion [35].

The study [36] is dedicated to solving the problem of synthesis of the optimal current controller operating under stochastic conditions [36]. Despite the advantage of this approach, namely, the simplicity of practical implementation of the algorithm, the question of control quality remains open. The controller parameters are calculated on the basis of the energy efficiency criterion for the specified design of the controller. However, they are optimal for the specified design only. Hence, this is not necessarily an optimal solution in terms of the quality of the control.

This weakness can be eliminated by synthesis of the optimal controller having an arbitrary design [37]. In case of this approach to the design of optimal controllers, it is the controller design that is subject to optimization, and its parameters are calculated specifically for the resulting design of the controller. However, this approach to the design of optimal controllers leads to uncertainty. It is related to the necessity of solving a system of equations where there are more unknowns than the equations.

The study [38] is dedicated to the synthesis of the optimal controller using the maximum principle. For the controllers based on the criterion of maximum, the design is synthesized, and the optimal controller parameters are calculated. Despite the obviously correct approach to solving the task of synthesis of the optimal controller, the algorithm specified has an essential drawback. The drawback is related to the fact that at low values of the error signal at the input, the output signal of the controller changes according to the linear law. The signal reaches the maximum possible value at the controller output, i.e., the controller enters the saturation mode under the presence of significant values of the error signal at the input.

This drawback may be eliminated by synthesis of the optimal controller using the dynamic programming method [39]. This algorithm is effective for the design of optimal controllers, provided that there are no control-related limitations. In case of any limitations, the method becomes difficult to implement. This is due to the fact that non-zero initial conditions need to be entered into the system of differential equations describing the system performance. This prompts the necessity to solve the system of non-homogenous differential equations.

Optimal filtration methods may be used for the synthesis of optimal controllers under stochastic conditions. In the case of the deterministic control signal and stochastic interference, the Kalman–Bucy filter method is the most effective [40]. This filter is implemented for the purpose of writing down the transfer function of the system by using the state-space representation. It is the most effective when analyzing the performance of the system in the time domain.

However, vector systems of drive control in asynchronous motors are discrete. They are implemented by means of z-transformation, i.e., in the frequency domain. In the frequency domain, the controllers synthesized by using the Wiener–Hopf equation are

the most effective. These controllers are also the most effective under the conditions of stochasticity of both the control signal and the interference [41,42].

Hence, it is relevant to implement the synthesis of optimal current controller on the basis of the Wiener–Hopf equation for the vector control system for the traction drive in electric locomotives with asynchronous motors.

The purpose of the study was to perform the synthesis of an optimal current controller based on the Wiener–Hopf equation for the vector control system for traction drive in electric locomotives with asynchronous motors.

The following was implemented for the purpose of the specified objective:

- The structural scheme was obtained in the transfer functions of the control channel for the current of the vector control systems for the traction drives in the AC electric locomotives;
- The synthesis of design and parameters of optimal current controller was obtained by using the Wiener–Hopf equation for the vector control system for the traction drive in the electric locomotive with asynchronous motors;
- Modeling of the synthesized current controller performance under the condition of deterministic character of the control signal and stochastic 'white-noise'-type interference;
- Comparison of the resulting transient characteristic of the synthesized controller with the transfer characteristic of the PI controller that is used in vector control systems for the traction drive in the AC electric locomotives.

The study may be used when investigating the energy efficiency of traction drives in AC electric locomotives, the interaction between the catenary system and the ERS, and the optimization of the control systems for traction drives in electric locomotives.

2. Materials and Methods

The optimal current synthesis was performed for the vector control system for the traction drive with the asynchronous motor. The structural scheme of the vector control system is presented in the study [28]. The control scheme parameters are presented in relative units.

A structural scheme in the transfer functions was designed for the vector control system. Current control channels were identified in the scheme. Optimal current controllers were synthesized for the current control channels by using the Wiener–Hopf equation.

A simulation model of the current control channel with the synthesized current controller was developed in the MATLab software environment. The transient characteristic of the current control channel was obtained for the conditions where the deterministic signal acted as a control signal at the controller input, and the stochastic 'white-noise'-type signal acted as an interference.

The transient characteristic was obtained for the initial control scheme for the same initial conditions. In this scheme, the PI controller was used as the current controller.

The transient characteristics obtained were compared in terms of the errors of the output control signals. The model was performed for the steady-state operation of the traction drive under its nominal operating conditions.

An AC electric locomotive with series DC-3 (ДС-3) asynchronous traction motor (Dnipro, Ukraine) was chosen as the object of the investigation. Type AD914U1 (АД914У1) asynchronous motors are used as traction motors in the electric locomotives of this series. Technical specifications of the AD914U1 (АД914У1) traction motor are presented in Table 1 [43].

Table 1. Parameters of AD914U1 (АД914У1) traction motor.

Parameter	Value
Power P, kW	1200
Phase-to-phase RMS voltage U_{nom}, V	1870
RMS value I_{nom}, A	450
Rated frequency of the supply voltage f, Hz	55.8
Number of phases n, pcs.	3
Number of pole pairs p_p	3
Nominal rotational speed n_r, rpm	1110
Efficiency η, %	95.5
Power factor cosφ, per unit	0.88
Active resistance of the stator winding r_s, Ω	0.0226
Active resistance of the rotor winding reduced to the stator winding r'_r, Ohm	0.0261
Stator winding leakage inductance $L_{\sigma s}$, Hn	0.00065
Rotor winding leakage inductance reduced to the stator winding, $L'_{\sigma r}$, Hn	0.00045
Total inductance of the magnetizing circuit L_{μ}, Hn	0.0194336
Moment of inertia of the motor J, kg·m^2	73

Current controller calculations were performed using the methodology presented in the study [44]. Calculations were performed using relative units. The calculation results are presented in Table 2.

Table 2. Calculation results for the basic values and parameters of the controller.

Parameter	Designation	Value
Current loop tuning coefficient X, r.u.	a_{Ix}	2
Current loop tuning coefficient Y, r.u.	a_{Iy}	2
Proportional coefficient of current controller X, r.u.	K_{pIx}	0.155
Integral coefficient of current controller X, r.u.	K_{iIx}	0.00922
Proportional coefficient of current controller Y, r.u.	K_{pIy}	0.155
Integral coefficient of current controller Y, r.u.	Ki_{Iy}	0.00922

The remaining parameters necessary for the synthesis of an optimal current controller were obtained as a result of the calculations and are provided below.

3. Calculations of the Optimal Current Controller Parameters by Using the Wiener–Hopf Equation

3.1. Definition of the Current Control Channels in the Transfer Functions of the Vector Control System

The structural scheme of the vector control system is presented in the study [28] and is depicted in Figure 1.

The following assumptions were made during the development of the above structural diagram:

1. In this paper, research on system operation of asynchronous motor asymmetric modes and on asynchronous motor asymmetric power supply system will not be conducted. Therefore, the induction motor model is chosen in x–y coordinates in order to avoid coordinate conversion;
2. The investigation will be carried out in steady-state mode of operation at motor shaft rotation frequency $\omega = \omega_{set}$. For this mode, the stator currents are fixed: $I_x^* = 1$ and $I_y^* = 0$, respectively.

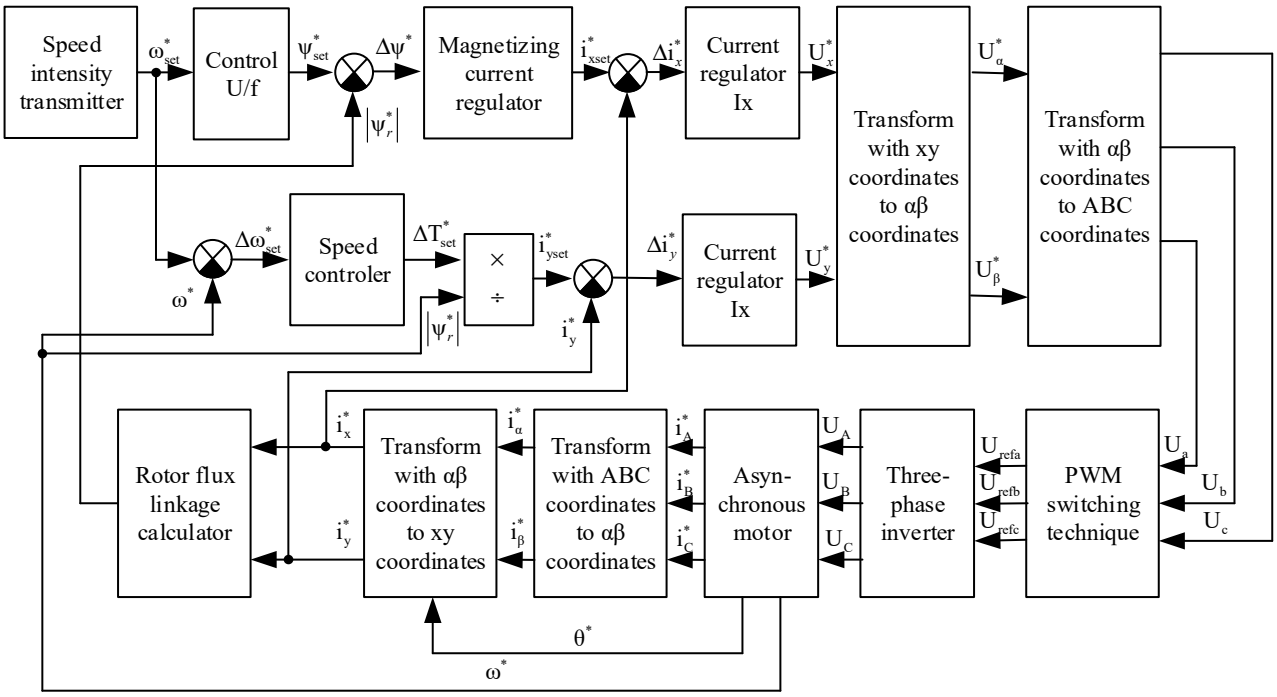

Figure 1. Structural scheme of the vector control system (* values presented in relative units of measurement).

Figure 1 depicts the structural scheme of the vector control system in the case of the common system of coordinates α-β oriented according to the flux linkage of the rotor in the system. Therefore, to define the structural scheme of the current control channel, the structural scheme of the 'Frequency converter—Asynchronous motor' system should be developed for the common system of coordinates α-β, which are oriented according to the flux linkage of the rotor.

Taking into account the recommendations for creating a vector control system with an induction motor represented in x–y coordinates [45], the structural diagram of the vector control system for an induction motor (Figure 1) is presented in transfer functions (Figure 2).

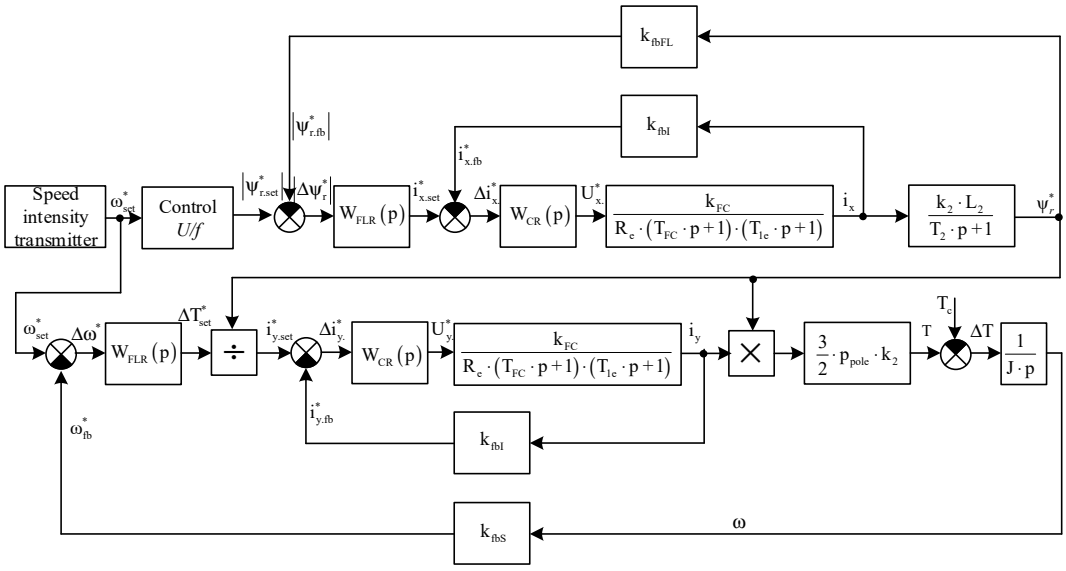

Figure 2. The structural scheme of the system 'Frequency converter—asynchronous motor' in the case of the common coordinate system of coordinates α-β, which are oriented according to the flux linkage of the rotor.

Figure 2 includes the following designations:

k_{fbI}, k_{fbFL}, and k_{fbS}—feedback coefficients for the current, flux linkage, and speed, respectively;
T_{1e}, T_2, and T_{FC}—time constants for the stator circuit, rotor circuit, and the frequency converter, respectively;
$W_{CR(p)}$, $W_{FL(p)}$, and $W_{SR(p)}$—transfer functions of the current controller, flux linkage controller, and speed, respectively;
k_2—coefficient of the electromagnetic link of the rotor;
k_{FC}—coefficient of the transfer function of the frequency converter;
R_{1e}—equivalent active resistance of the stator circuit.

The values indicated with the index * are used in relative units.

To synthesize a current regulator, a current transfer channel with a transfer $W(p)_C = i(p)/i_{set}(p)$ function for x and y coordinates should be identified. Figure 2 suggests that the transferred functions of the current control channels are the same for coordinates x–y. Given the assumption that studies are conducted for the mode $\omega = \omega_{set}$, for which the stator currents are fixed: $I_x^* = 1$ and $I_y^* = 0$ the structural diagram of the current transmission channel is shown in Figure 3.

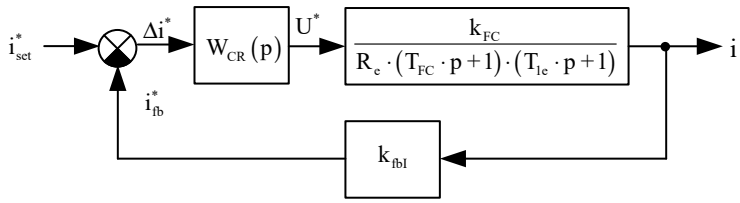

Figure 3. Structural scheme of the current control channels (* values presented in relative units of measurement).

For convenience of subsequent calculations, the following transformations of the structural scheme were performed (Figure 3):

- The scheme (Figure 3) with a non-unique transfer function of feedback (k_{fbI}) was transformed into the structural scheme with a unique feedback connection (Figure 4);
- In the scheme (Figure 4), the interferences acting on the current sensors in the stator circuit was depicted as signal f;
- The signal having the specified stator current value (I_{1set}) was designated as x, and the output signal of stator current (I_1) was designated as y.

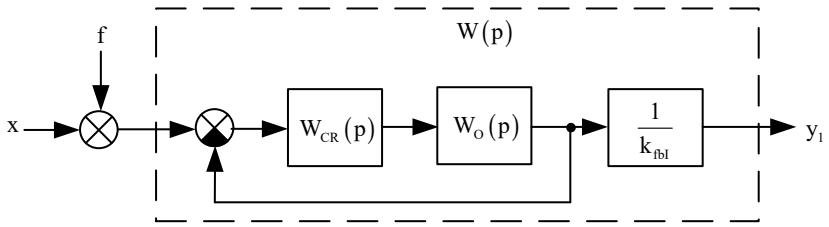

Figure 4. Design structural scheme of the current control channels.

The design scheme for the current control channel resulting from the transformations above is presented in Figure 4.

Transfer function of the control object in the design scheme:

$$W'_O(p) = \frac{k_{fbI} \cdot k_{fFC}}{R_{e1} \cdot (T_{FC} \cdot p + 1) \cdot (T_{e1} \cdot p + 1)} \quad (1)$$

In expression (1), active resistance of the stator circuit was defined by expression:

$$R_{e1} = r_s + r'_r \cdot k_2^2 \quad (2)$$

where r_s = 0.0226 Ω—active resistance of the stator phase (Table 1); r'_r = 0.0261 Ω—active resistance of the rotor phase reduced to the stator (Table 1); $k_2 = L_\mu/(L'_{\sigma r} + L_\mu)$ = 0.9774—coefficient of the electromagnetic link of the rotor; L_μ = 0.0194336 Hn—inductance of the magnetic circuit of the motor (Table 1); and $L'_{\sigma r}$ = 0.00045 Hn—inductance of the rotor phase leakage reduced to the stator (Table 1).

The time constant of the stator circuit in Equation (1) was determined by using formula:

$$T_{e1} = \frac{k_2 \cdot L_{\sigma e}}{R_{e1}} = 0.023 \text{ s} \tag{3}$$

where $L_{\sigma e}$—equivalent inductance of the motor leakage.

$$L_{\sigma e} = L_{\sigma s} + L'_{\sigma r} + \frac{L_{\sigma s} \cdot L'_{\sigma r}}{L_\mu} = 0.001115 \text{ Hn} \tag{4}$$

where $L_{\sigma s}$—inductance of the stator winding leakage.

Time constant of the frequency converter in Equation (1) was determined by using formula:

$$T_{FC} = a_T \cdot T_{e1} = 2 \times 0.023 = 0.046 \text{ s} \tag{5}$$

where a_T—current controller tuning coefficient. It is usually accepted that a_T = 2.

The transfer coefficient of the frequency converter is determined by expression:

$$k_{FC} = \frac{I_{snom}}{I_1} = \frac{450}{1} = 450 \text{ A} \tag{6}$$

where I_{snom} = 450 A—nominal value of the stator current (Table 1) and I_1—nominal current value at the current controller output. The vector control scheme (Figure 1) was implemented in relative units, I_1 = 1 A.

The feedback coefficient for the current:

$$k_{fbI} = \frac{1}{I_{snom}} = \frac{1}{450} = 0.0022 \, 1/\text{A} \tag{7}$$

The transfer scheme of the current control circuit is therefore the following:

$$W(p) = \frac{W'_O(p) \cdot W_{FC}(p)}{1 + W'_O(p) \cdot W_{FC}(p)} \cdot \frac{1}{k_{fbI}} = \frac{k_{fFC}}{1 + k_{fbI} \cdot R_{e1} \cdot W'_O(p) \cdot W_{FC}(p)} \tag{8}$$

To determine the structure and parameters of the optimal current controller using the Wiener–Hopf equation, it is necessary to determine the signal parameters and the interferences that act at the controller input (Figure 4).

3.2. Determination of the Parameters of the Signal and the Interferences That Act at the Controller Input

Reference signal $x(t) = \alpha \cdot \sin(\omega \cdot t + \beta)$ and 'white-noise'-type interference f(t) act at the system input (Figure 4) [46]. In the performed analysis, it was found that vector drive control systems with asynchronous motors are discrete systems. They are implemented using the z-transformation, i.e., in the frequency domain. In the frequency domain, the most effective regulators are those synthesized using the Wiener–Hopf equation. Additionally, the regulators synthesized with the Wiener–Hopf equation are the most effective under the condition of stochasticity of both the control signal and the disturbance [41,42].

According to the methodology for the calculation of the optimal controller using the Wiener–Hopf equation [41,42], it is necessary to obtain the spectral densities of the control signal and of the interference. To determine the spectral density of the signal at the controller input x(t) taking into account the structure of the vector control system, the following operations had to be performed:

- Time dependences of the phase currents of the stator had to be obtained for the model;
- The resulting dependences had to be transformed for the system of coordinates x–y;
- The signal parameters had to be calculated.

Calculation of the controller parameters is performed for the steady-state nominal operation of the control system. As a result, to reduce the number of coordinate transformations, the following hypothesis was established: it can be assumed, with a certain minor error, that the current at the input of the current control channel (Figure 3) is equal to phase A stator current of the traction motor. Studies [43,47] propose the model of АД914У1 asynchronous motor in three-phase coordinates. This model provided the time diagrams of the stator current and phase voltage of phase A for the steady-state mode (Figure 5a). These time diagrams were used to determine the parameters of signal x(t): amplitude α = 450 A, phase shift between the voltage and the current β = 1.4 rad. Using this model, time diagrams of the stator current and phase voltage of phase A for steady state mode were obtained (Figure 5a). They are used to determine the parameters of the signal I_{sa}: amplitude A = 450 A, phase shift between voltage and current φ = 1.4 rad. The current feedback coefficient is equal to the inverse of the nominal current. In other words, a current whose amplitude is equal to $\alpha = A \cdot k_{fbI} = 450 \cdot 1/450 = 1$ relative units, that is, the reduced value of the current amplitude is obtained. The induced current phase value is defined as $\beta = \varphi/(2 \cdot \pi) = 0.223$ relative units. In other words, the expression for the feedback current is $y = \alpha \cdot \sin(\omega \cdot t + \beta)$.

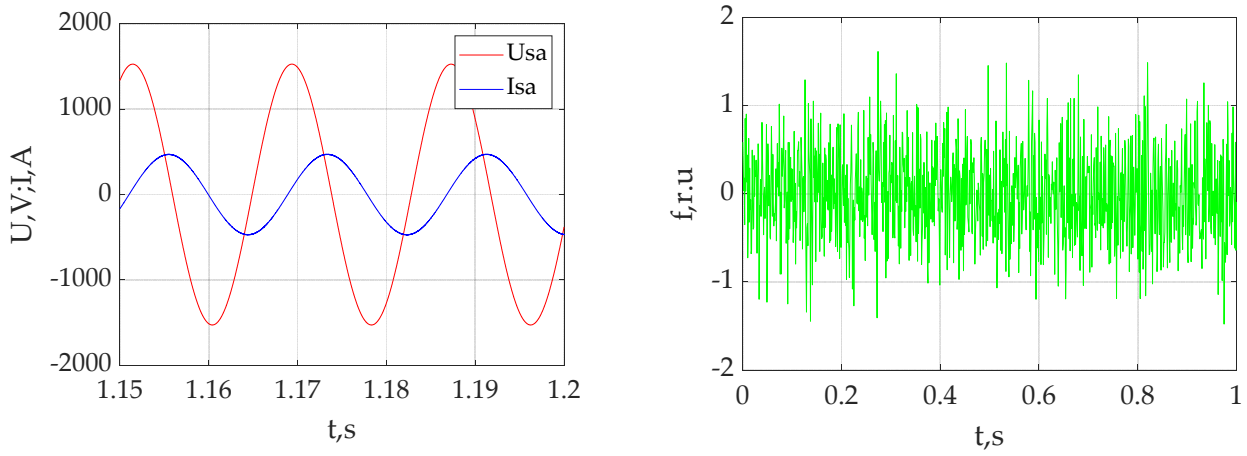

Figure 5. Time diagrams: (**a**) of the stator current and phase voltage of phase A for the steady−state mode; (**b**) 'white-noise'-type of interferences.

The 'white-noise'-type signal parameters were determined on the basis of the following considerations. The mathematical expectation of the 'white-noise'-type signal was equal to zero [46]. Lower 'white noise' dispersion was chosen than the tolerable control error equal to 5%. The chosen value of the mean squared deviation of the interference was N = 0.3375. Then, the dispersion of interference N^2 = 0.114. Time diagram of the interference signal is provided in Figure 5b. Since the noise is fed to the current regulator input, which receives the reduced stator current value expressed in relative units, the noise from the current sensor f is also expressed in relative units.

Spectral density of the reference signal was calculated by using formula [48]:

$$S_y(\omega) = \frac{1}{\sqrt{2 \cdot \pi}} \cdot \int_{-\infty}^{\infty} y(t) \cdot e^{-j\omega \cdot t} dt = \frac{1}{\sqrt{2 \cdot \pi}} \cdot \int_{-\infty}^{\infty} (\alpha \cdot \sin(\omega \cdot t + \beta))^2 \cdot e^{-j\omega \cdot t} dt = \frac{\alpha^2}{\omega^2 + \beta^2} \quad (9)$$

Spectral density of the interference was calculated by using formula [49]:

$$S_f(\omega) = N^2 \tag{10}$$

A hypothesis was proposed under the condition of synthesis of the optimal current controller, namely, that the signals y(t) and f(t) are not correlated.

3.3. Determination of the Structure and Parameters of the Optimal Current Regulator

Under the condition of synthesis of the optimal current regulator, the closed-loop system is required to perform a certain Z(p) function using reference signal Y(p) in accordance with transfer function H(p):

$$Z(p) = H(p) \cdot Y(p) \tag{11}$$

Error of the control adjusted for interference F(p):

$$e(p) = Z(p) - Y_1(p) \tag{12}$$

For this purpose, the weighting function for the closed-loop system g*(t) was determined to ensure that the mean squared error has the lowest value:

$$\bar{e}^2 = \lim_{T \to \infty} \frac{1}{T} \cdot \int_{-\infty}^{t} e^2 dt = \left| \overline{z(t) - y_1(t)} \right|^2 \to \min \tag{13}$$

where $z(t)$—the specified function and $y_1(t)$—the reference signal.

This means that the synthesized system would provide maximum suppression of the interference f(t) in the reference signal. The Wiener–Hopf procedure was used to find the transfer function of the optimal controller. For this purpose, the weighting function of the system has the following expression:

$$g(t, \tau) = g^*(t, \tau) + \varepsilon \cdot \eta(t, \tau) \tag{14}$$

η(t,τ)—some function; ε—small parameter.

Reference value $y_1(t)$ was obtained by using the convolution function:

$$y_1(t) = \int_{-\infty}^{t} [g^*(t, \tau) + \varepsilon \cdot \eta(t, \tau)] \cdot y_1(\tau) dt \tag{15}$$

Then, the filtration error is:

$$\bar{e}^2 = M\left\{ |z(t) \cdot y_1(t)|^2 \right\} = M\left\{ \left| z(t) \cdot \int_{-\infty}^{t} [g^*(t, \tau) + \varepsilon \cdot \boldsymbol{\eta}(t, \tau)] \cdot y_1(\tau) d\tau \right|^2 \right\} \tag{16}$$

where M[·]—the operation of mathematical expectation.

Optimal weighting functions were determined based on condition:

$$\frac{\partial \bar{e}^2}{\partial t} = 0 \text{ near the point } \varepsilon = 0 \tag{17}$$

$$\frac{\partial \bar{e}^2}{\partial \varepsilon} = 2 \cdot M\left\{ \left| z(t) - \int_{-\infty}^{t} g^*(t, \tau) \cdot y_1(\tau) d\tau - \int_{-\infty}^{t} \eta(t, \tau) \cdot y_1(\tau) d\tau \right| \right\} \tag{18}$$

In the integrand of the second integral (18), τ was replaced with ξ. Furthermore, the non-random character of the function η(t,ξ) was taken into account. This enabled the authors to remove it under operator M[·]:

$$\frac{\partial \bar{e}^2}{\partial \varepsilon} = \int_{-\infty}^{t} \eta(t,\xi)\cdot\left\{ M[z(t)\cdot y_1(\xi)] - M\left[\int_{-\infty}^{t} g^*(t,\tau)\cdot y_1(\xi)\cdot y_1(t)d\tau\right]\right\} d\xi \tag{19}$$

Taking into account the non-random character of g*(t,τ) and the fact that η(t,τ) = 0, the following was obtained:

$$M[z(t)\cdot y_1(\xi)] = \int_{-\infty}^{t} g^*(t,\tau)\cdot y_1(\xi)\cdot y_1(t)d\tau \tag{20}$$

Considering the character of operation M[·], the Wiener–Hopf equation was obtained:

$$R_{zy}(t,\xi) = \int_{-\infty}^{t} g^*(t,\tau)\cdot R_y(\tau,\xi)d\tau \tag{21}$$

where $R_{zy}(t,\xi)$—cross-correlation function of signals z(t) and $y_1(t) = x(t) + f(t)$; $R_y(\tau,\xi)$—correlation function of signal$y_1(t)$; and g*(t,τ)—weighting function of the optimal closed-loop system.

Frequency transfer function of the Wiener filter was obtained from expression (21):

$$W_{opt}(j\omega) = \frac{1}{2\cdot\pi\cdot\psi(j\omega)}\cdot\int_{0}^{\infty} e^{-j\omega t}dt\cdot\int_{-\infty}^{\infty}\frac{S_{zy}(j\omega)}{\psi(-j\omega)}\cdot e^{j\omega t}d\omega \tag{22}$$

where:

$$S_{zy}(j\omega) = S_{zy}(j\omega) + S_{zf}(j\omega) \tag{23}$$

where $S_{zy}(j\omega)$—cross-spectral density of the wanted signal and the input signal; and $S_{zy}(j\omega)$, $S_{zf}(j\omega)$—cross-spectral densities of the signals, respectively.

The spectral density of the composite signal $y_1(t)$ was subjected to the factorization procedure:

$$S_{y1}(j\omega) = \psi(j\omega)\cdot\psi(-j\omega) \tag{24}$$

where:

$$S_{y1}(j\omega) = S_y(j\omega) + S_f(j\omega) + S_{yf}(j\omega) + S_{fy}(j\omega) \tag{25}$$

Reference signal y(t) and interference f(t) are not correlated to each other, so:

$$S_{yf}(j\omega) = S_{fy}(j\omega) = S_{zy}(j\omega) = 0 \tag{26}$$

Spectral density $S_{y1}(j\omega)$ is an even function of frequency ω. It can be depicted as follows:

$$S_{y1}(\omega) = \frac{b_0 + b_1\cdot\omega^2 + , \ldots , + b_m\cdot\omega^{2m}}{a_0 + a_1\cdot\omega^2 + , \ldots , + a_n\cdot\omega^{2n}} \tag{27}$$

where $a_0, a_1, \ldots, a_n$—coefficients at even degrees of the denominator of the function and $b_0, b_1, \ldots, b_n$—coefficients at even degrees of the numerator of the function.

From which:

$$\begin{cases} \psi(j\omega) = A\cdot\frac{(\omega-\gamma_1)\cdot(\omega-\gamma_2)\cdot,\ldots,\cdot(\omega-\gamma_m)}{(\omega-\lambda_1)\cdot(\omega-\lambda_2)\cdot,\ldots,\cdot(\omega-\lambda_n)}, \\ \psi(-j\omega) = A\cdot\frac{(\omega+\gamma_1)\cdot(\omega+\gamma_2)\cdot,\ldots,\cdot(\omega+\gamma_m)}{(\omega+\lambda_1)\cdot(\omega+\lambda_2)\cdot,\ldots,\cdot(\omega+\lambda_n)}. \end{cases} \tag{28}$$

where γ_i, λ_j—zeros and pluses of function $S_{y1}(j\omega)$:

$$A = \sqrt{\frac{b_m}{a_n}} \tag{29}$$

Condition H(p) = 1 was accepted. This condition corresponds to the synthesis of the optimal servo system. As a result, Equation (22) became simpler:

$$W_{opt}(j\omega) = \frac{B(j\omega)}{\psi(j\omega)} \tag{30}$$

where:

$$B(j\omega) = \sum_{i=1}^{r} \frac{a_i}{\omega - \eta_i} \tag{31}$$

where η_i—poles of function:

$$\eta_i = \frac{S_y(j\omega)}{\psi(-j\omega)} \tag{32}$$

Located in the upper half plane:

$$a_i = \left[(\omega - \eta_\iota)\cdot\frac{S_y(j\omega)}{\psi\,(-j\omega)}\right]_{\omega=\eta_i} \tag{33}$$

Spectral density of the output signal under the conditions of absence of correlation between reference signal y(t) and interferences f(t) in accordance with Equation (23) is determined as:

$$S_y(\omega) = \frac{\alpha^2}{\omega^2 + \beta^2} + N^2 \approx N^2\cdot\frac{\omega^2 + \alpha^2}{\omega^2 + \beta^2} \tag{34}$$

Factorization of expression (34) is as follows:

$$S_y(\omega) = N\cdot\frac{\omega + j\alpha}{\omega + j\beta}\cdot N\cdot\frac{\omega - j\alpha}{\omega - j\beta} \tag{35}$$

where:

$$\psi(-j\omega) = N\cdot\frac{\omega + j\alpha}{\omega + j\beta}, \tag{36}$$

$$\psi(j\omega) = N\cdot\frac{\omega - j\alpha}{\omega - j\beta}. \tag{37}$$

whereas signals y(t) and f(t) are not correlated, then:

$$S_y(\omega) = \frac{\alpha^2}{\omega^2 + \beta^2} = \frac{\alpha^2}{(\omega + j\beta)\cdot(\omega - j\beta)} \tag{38}$$

In accordance with expression (32):

$$S_y(\omega)\cdot\frac{1}{\Psi(-j\omega)} = \frac{\alpha^2}{(\omega + j\beta)\cdot(\omega - j\beta)}\cdot\frac{\omega + j\beta}{N\cdot(\omega + j\alpha)} = \frac{\alpha^2}{N\cdot(\omega + j\alpha)\cdot(\omega - j\beta)} \tag{39}$$

The function has two poles: $\eta_1 = j\beta$ and $\eta_1 = -j\alpha$. Pole $\eta_1 = j\beta$ is located in the upper half plane. Then:

$$a_i = \left[(\omega - j\beta)\cdot\frac{\alpha^2}{N\cdot(\omega + j\alpha)\cdot(\omega - j\beta)}\right]_{\omega=j\beta} = \frac{\alpha^2}{jN\cdot(\beta + \alpha)} \tag{40}$$

Considering expression (31), the following was found:

$$B(j\omega) = \frac{\alpha^2}{jN\cdot(\beta+\alpha)\cdot(\omega-j\beta)} \quad (41)$$

Using Equation (30), the frequency transfer function of the optimal system was obtained:

$$W_{opt}(j\omega) = \frac{B(j\omega)}{\psi(j\omega)} = \frac{\alpha^2}{jN\cdot(\beta+\alpha)\cdot(\omega-j\beta)}\cdot\frac{(\omega-j\beta)}{N\cdot(\omega-j\alpha)} = \frac{\alpha^2}{jN^2\cdot(\beta+\alpha)\cdot(\omega-j\alpha)} = \frac{k_1}{T\cdot j\omega+1}, \quad (42)$$

where:

$$k_1 = \frac{\alpha}{N^2\cdot(\beta+\alpha)} = \frac{1}{0.3375^2\cdot(0.223+1)} = 8.752,\ \text{r.u.};\ T = \frac{1}{\alpha} = 1,\ \text{r.u.} \quad (43)$$

Then, the structure of essentially optimal current control channel controller of the vector system for maximum suppression of the action of interference f(t) is the following:

$$W_{CRopt}(p) = \frac{W_{CRopt}(p)}{W_O(p)\cdot[1-W_{CRopt}(p)]} = \frac{k_1\cdot(1+k_{fbI}\cdot R_{e1}\cdot(T_{FC}\cdot p+1)\cdot(T_1\cdot p+1))}{k_{FC}\cdot(T_1\cdot p+1-k_1)}. \quad (44)$$

Hence, expression (44) determines the structure of the optimal controller.

3.4. Simulation Results

The structural scheme of the current control channel (Figure 4) was implemented in the MATLab program environment for the basic vector control and the system of vector control with the optimal current controller. Simulation of the performance of the control scheme was performed in the presence of the reference signal y(t) and interference f(t) at the controller input. The time diagrams of the stator current of phase A of the traction motor were obtained for the basic control scheme and for the control scheme with the optimal controller (Figure 6).

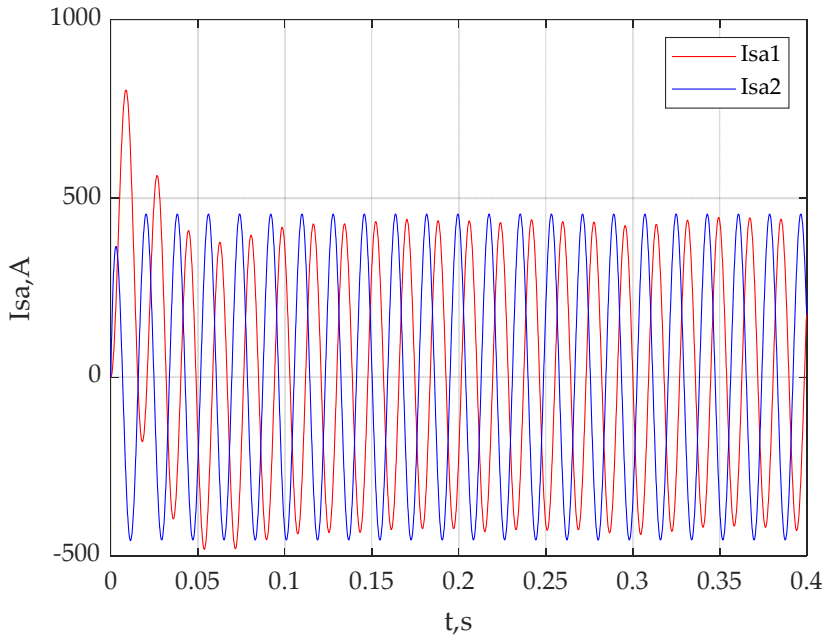

Figure 6. Time diagrams of stator current of phase A of the traction motor: I_{sa1}—of the basic scheme of vector control; I_{sa2}—of the control system with the optimal controller.

As suggested in Figure 6, the system of vector control with the optimal current controller is more resistant to the action of interferences.

To compare the quality indicators of control of both the systems, the transient characteristics of the basic system of vector control and of the system with the optimal controller were obtained. For this purpose, a unit step-type signal was fed to the input of the both systems (45) under the condition of absence of the interference current at the controller input:

$$x(t) = \begin{cases} 0, \text{ if } t < 0, \\ 1, \text{ if } t \geq 0. \end{cases} \quad (45)$$

The transient functions of the basic vector control system (I_{sa1}) and the vector system with the optimal controller (I_{sa2}) are presented in Figure 7a. The time values of the transient process for the basic system (t_{st1}) and the system with optimal current controller (t_{st2}), the steady-state value of the stator current (I_{sa1st}) and (I_{sa2st}), and the maximum value of the stator current (I_{sa1max}) and (I_{sa2max}), respectively, were determined based on the transient characteristics. The results are presented in Table 3. The overshooting of both systems was calculated using the formula:

$$\sigma = \frac{I_{samax} - I_{sast}}{I_{sast}} \cdot 100\%. \quad (46)$$

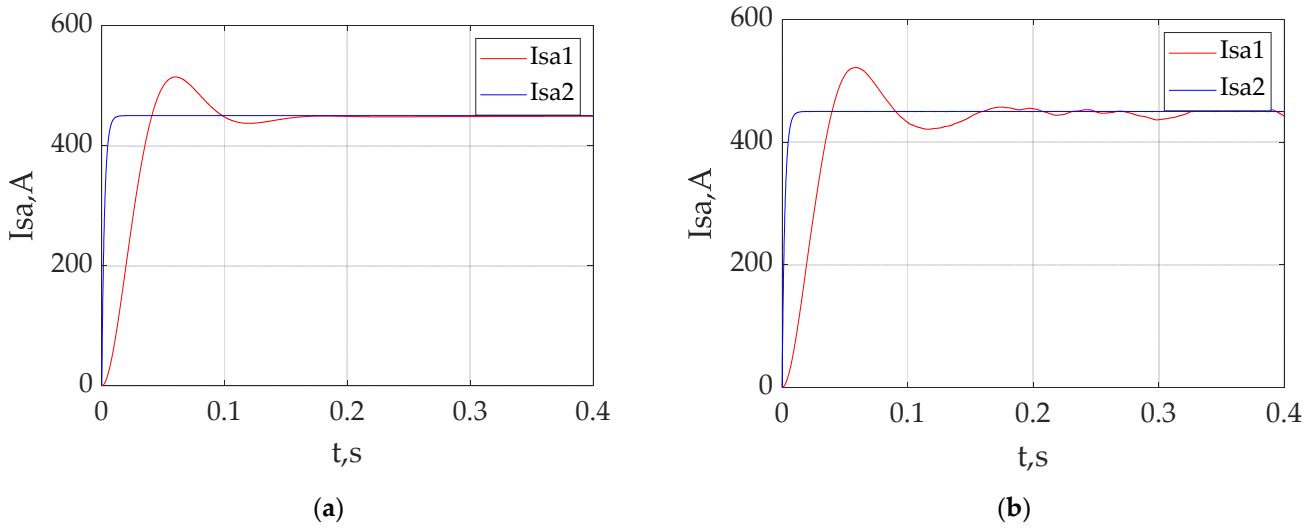

Figure 7. Transient functions: (**a**) under the absence of an interference at the current controller input (of the basic control system (I_{sa1}) and system with the optimal current controller (I_{sa2st})); (**b**) under the presence of an interference at the current controller input (of the basic control system (I_{sa1}) and system with the optimal current controller (I_{sa2st})).

Table 3. The results of comparison of the control quality of the basic system versus the system with optimal controller.

Parameter	Designation	Unit of Measurement	Value	
			Basic System	System with Optimal Controller
Time of transient process	t_{st}	s	0.166	0.0138
Steady-state values	$I_{sa.st}$	A	450	450
Maximum value	$I_{sa.max}$	A	514.4	450
Overshooting	σ	%	14.3	0
Control accuracy	ε	%	1.3151	0.0134

The results of the overshoot calculations are presented in Table 3.

To determine the precision of control of both control systems, transient functions were obtained under the condition of the presence of the 'white-noise'-type of interference controllers at the input. Transient functions under the condition of interferences of the basic control system (I_{sa1}) and the system with the optimal current controller (I_{sa2st}) are presented in Figure 7b.

The control errors were calculated for the steady-state mode of both systems using formula:

$$\varepsilon = \frac{\frac{1}{N-1} \cdot \sum_{i=0}^{N} (I_{sast} - I_{sai})^2}{I_{sast}} \cdot 100\% \quad (47)$$

where: I_{sast}—steady-state value of stator current; N—number of samples.

The results of calculations are presented in Table 3.

The control quality parameter, such as the time of the oscillatory process, was not taken into account due to the lack of its relevance in the investigation. Since there is no overshoot in the proposed regulator as opposed to the basic regulator (Figure 7), this means that the current control channel with the proposed regulator has an infinite phase stability margin.

4. Discussion

In the present study, the deterministic signal was used as the reference signal and the stochastic signal was used as the interference.

This circumstance can be explained by the following two factors:

1. Objective difficulties in obtaining the experimental data on the dependence of the stator current of the traction motor in the case of the stochastic character of the change of the phase voltage;
2. Performance of the existing models of the asynchronous motor under the stochastic character of change of the phase voltage was not analyzed. The results of the simulation of performance of the asynchronous traction drive with the vector control system may be flawed.

The second factor also explains the choice of only the current control channel of the vector control system for the investigation.

The quality of the current control channel of the vector control system for the asynchronous traction drive was determined according to its transient characteristics under the condition of absence of interferences at the input (Figure 7a). Comparison of the quality indicators of the basic system and of the system with the optimal controller (Table 3) showed that:

- The steady-state value of the output signal of the both systems was equal to 450 A. This value corresponded to the value of the nominal phase current of the asynchronous traction motor;
- The speed of response of the system with the optimal controller was higher than that of the basic system. Time of the transient process (Table 3) of the system with optimal controller t_{st1} = 0.0138 s, of the basic system—t_{st1} = 0.166 s;
- Transient function of the system with the optimal controller was free from oscillations. The basic system had oscillations. Value of overshooting of the basic system was 14.3%.

The accuracy of the overshooting of the current control channels was determined based on the transient functions of the systems in the presence of 'white-noise'-type interference at the controller input (Figure 7b). The comparison of simulation results (Table 3) showed that the system with the optimal controller had a 1.3% lower control error than the basic system. This fact suggests that the power loss caused by control interferences is 1.69% lower in the traction drive with the optimal controller than in the drive with the basic control system. This can be supported by the phase current diagrams of the stator (Figure 6) under the presence of interferences at the controller input. For the steady-state mode, the phase current value of the stator of the traction motor with the basic control system was 444 A, with the optimal controller—450 A.

There are some important caveats to the study that deserve mention:

1. The current control channel models of the control circuits were based on the assumption that the control signal at the input of the current controllers is a deterministic signal;
2. The character of load variation was not taken into account (it can have a stochastic nature);
3. The investigations were carried out for the mode of operation, when the value of the shaft rotation speed is equal to the value of the given rotation speed;
4. The optimal current controller will work correctly for the set operating mode of the traction drive system. This fact is related to the condition that the parameters of the optimal current regulator depend on the values of stator current and noise variance. During transients, these parameters change.

Nonetheless, it should be taken into account that the models of the current control channels were based on the assumption that the reference signal at the current controller input was a deterministic signal. This factor implies certain limitations to the application of the model developed. To account for this factor, additional investigations must be conducted. At the same time, the authors realize the difficulties related to retrieval of the experimental data under the conditions of operation of an electric locomotive.

In the process of work on the present paper, the authors encountered objective difficulties related to the absence of any possibility to conduct a full-scale experiment and retrieve valid experimental data. This is related to the fact that the control systems are essentially microprocessor systems by design. To record the experimental oscillograms of the signals at the current control input, it is necessary to obtain permission from the respective manufacturers of the systems. This is difficult to implement as this is related with trade secrets.

Further work to improve on these new developments is suggested:

1. Investigation of the influence of the stochastic nature of voltage changes in the contact network on the supply voltage of the autonomous voltage inverter;
2. Investigation of the influence of thermal noise of the autonomous voltage inverter on the operation of the vector control system;
3. Investigation of the thermal noise of traction motor windings on the operation of the vector control system;
4. Investigation of the stochastic nature of the traction drive load on the operation of the vector control system;
5. Development of a current regulator, whose parameters are adapted to the operating conditions of the locomotive.

5. Conclusions

1. The structural scheme was obtained in the transfer functions of the current control channel of the vector control systems for the asynchronous traction drives in the AC electric locomotives. Spectral densities of the reference signal and of the interference at the current controller input were calculated.
2. The design synthesis was performed, and parameters of optimal current controller parameters were obtained by using the Wiener–Hopf equation for the vector control system for the traction drive in the electric locomotive with the asynchronous motor.
3. Simulation of the current control channel of the basic vector control system and of the system with the optimal controller was performed.
4. The transient characteristics of the current control channels of the basic control system and the optimal controller were obtained under the condition of absence of interferences at the controller input. Comparison of the time of the transient processes showed that:
   - The speed of response of the system with the optimal controller was higher by 1.3 s compared to the basic control system;
   - Transient characteristic of the system with the optimal controller was free from oscillations. The oscillations were present in the transient characteristic of the basic system. The overshoot of the basic system was equal to 14.3%.
   - The steady-state value of the transient function of the both systems was 450 A, which corresponded to the nominal value of the phase current of the stator of the traction motor.

The accuracies of control of the two systems were calculated on the basis of the transient characteristics of the current control channels under the condition of the presence of 'white noise' interferences at the controller input. The accuracy of the control of the system with the optimal controller was higher by 1.3% than that of the basic system.

Analysis of the time diagrams of the phase currents of the traction drive showed that the presence of interferences at the input of the current controller in the optimal controller did not influence the value of the phase current of the motor stator. In the basic system, the value of the phase current of the stator was lower by 1.3% compared to the operation without interferences. This fact suggests that the power loss is 1.69% lower in the traction drive with the optimal controller than in the traction drive with the basic control system.

6. Patents

Implementation of the present study was financially supported by the Ministry of Education and Science of Ukraine under the framework of the R&D project 'Improvement of energy efficiency of the railway rolling stocks on the basis of the resource-saving technologies and intelligent power systems' (state registration number 0120U101912).

Author Contributions: Conceptualization, methodology, and investigation S.G., V.T., S.S. and B.L.; investigation, writing—review and editing, S.G., V.L. and R.K.; formal analysis, writing—review and editing, R.M. and A.K.; investigation, S.G., V.T., S.S. and B.L. All authors have read and agreed to the published version of the manuscript.

Funding: This publication was realized with the support of Operational Program Integrated Infrastructure 2014–2020 of the project: Innovative Solutions for Propulsion, Power, and Safety Components of Transport Vehicles, code ITMS 313011V334, co-financed by the European Regional Development Fund.

Institutional Review Board Statement: Not applicable.

Informed Consent Statement: Not applicable.

Data Availability Statement: Not applicable.

Conflicts of Interest: The authors declare no conflict of interest.

References

1. Kostin, M.; Mishchenko, T.; Hoholyuk, O. Fryze Reactive Power in Electric Transport Systems with Stochastic Voltages and Currents. In Proceedings of the 2020 IEEE 21st International Conference on Computational Problems of Electrical Engineering (CPEE), Online, 16–19 September 2020; pp. 1–4. [CrossRef]
2. Feng, D.; Yang, C.; Cui, Z.; Li, N.; Sun, X.; Lin, S. Research on Optimal Nonperiodic Inspection Strategy for Traction Power Supply Equipment of Urban Rail Transit Considering the Influence of Traction Impact Load. *IEEE Trans. Transp. Electrif.* **2020**, *6*, 1312–1325. [CrossRef]
3. Goolak, S.; Tkachenko, V.; Bureika, G.; Vaičiūnas, G. Method of Spectral Analysis of Traction Current of AC Electric Locomotives. *Transport* **2021**, *35*, 658–668. [CrossRef]
4. Kostin, M.; Nikitenko, A.; Mishchenko, T.; Shumikhina, L. Electrodynamics of Reactive Power in the Space of Inter-Substation Zones of AC Electrified Railway Line. *Energies* **2021**, *14*, 3510. [CrossRef]
5. Morris, J.; Robinson, M.; Palacin, R. Use of Dynamic Analysis to Investigate the Behaviour of Short Neutral Sections in the Overhead Line Electrification. *Infrastructures* **2021**, *6*, 62. [CrossRef]
6. Mariscotti, A. Critical Review of EMC Standards for the Measurement of Radiated Electromagnetic Emissions from Transit Line and Rolling Stock. *Energies* **2021**, *14*, 759. [CrossRef]
7. Song, Y.; Wang, H.; Liu, Z. An Investigation on the Current Collection Quality of Railway Pantograph-Catenary Systems with Contact Wire Wear Degradations. *IEEE Trans. Instrum. Meas.* **2021**, *70*, 1–11. [CrossRef]
8. Mariscotti, A. Data sets of measured pantograph voltage and current of European AC railways. *Data Brief* **2020**, *30*, 105477. [CrossRef]
9. Song, Y.; Antunes, P.; Pombo, J.; Liu, Z. A methodology to study high-speed pantograph-catenary interaction with realistic contact wire irregularities. *Mech. Mach. Theory* **2020**, *152*, 103940. [CrossRef]
10. Mikhailov, E.; Sapronova, S.; Tkachenko, V.; Semenov, S.; Smyrnova, I.; Kholostenko, Y. Improved solution of guiding of railway vehicle in curves. In Proceedings of the 23th International Scientific Conference "Transport Means", Palanga, Lithuania, 2–4 October 2019; pp. 916–921. Available online: https://transportmeans.ktu.edu/wp-content/uploads/sites/307/2018/02/Transport-means-2019-Part-2.pdf (accessed on 20 December 2021).

11. Grebennikov, N.; Kharchenko, P. Development of a Computer Model of a Passenger Train Using Data from Devices for Train Operation Parameters Registration. In Proceedings of the 2021 International Conference on Industrial Engineering, Applications and Manufacturing (ICIEAM), Sochi, Russia, 17–21 May 2021; pp. 908–913. [CrossRef]
12. Babyak, M.; Keršys, R.; Neduzha, L. Improving the Dependability Evaluation Technique of a Transport Vehicle. In Proceedings of the 24th International Scientific Conference "Transport Means", Palanga, Lithuania, 30 September–2 October 2020; pp. 646–651. Available online: http://eadnurt.diit.edu.ua/jspui/handle/123456789/12287 (accessed on 20 December 2021).
13. Zhou, Z.; Chen, Z.; Spiryagin, M.; Wolfs, P.; Wu, Q.; Zhai, W.; Cole, C. Dynamic performance of locomotive electric drive system under excitation from gear transmission and wheel-rail interaction. *Veh. Syst. Dyn.* **2021**, 1–23. Available online: https://www.tandfonline.com/doi/full/10.1080/00423114.2021.1876887 (accessed on 20 December 2021). [CrossRef]
14. Goolak, S.; Sapronova, S.; Tkachenko, V.; Riabov, I.; Batrak, Y. Improvement of the model of power losses in the pulsed current traction motor in an electric locomotive. *East. Eur. J. Enterp. Technol.* **2020**, *6*, 38–46. [CrossRef]
15. Rouamel, M.; Gherbi, S.; Bourahala, F. Robust stability and stabilization of networked control systems with stochastic time-varying network-induced delays. *Trans. Inst. Meas. Control* **2020**, *42*, 1782–1796. [CrossRef]
16. Wang, B.; Zhu, Q. Stability Analysis of Discrete-Time Semi-Markov Jump Linear Systems. *IEEE Trans. Autom. Control* **2020**, *65*, 5415–5421. [CrossRef]
17. Jiao, T.; Zong, G.; Pang, G.; Zhang, H.; Jiang, J. Admissibility analysis of stochastic singular systems with Poisson switching. *Appl. Math. Comput.* **2020**, *386*, 125508. [CrossRef]
18. Ronanki, D.; Singh, S.A.; Williamson, S.S. Comprehensive Topological Overview of Rolling Stock Architectures and Recent Trends in Electric Railway Traction Systems. *IEEE Trans. Transp. Electrif.* **2017**, *3*, 724–738. [CrossRef]
19. Pugachev, A. Efficiency increasing of induction motor scalar control systems. In Proceedings of the 2017 International Conference on Industrial Engineering, Applications and Manufacturing (ICIEAM), St. Petersburg, Russia, 16–19 May 2017; pp. 1–5. [CrossRef]
20. Costa, C.A.; Nied, A.; Nogueira, F.G.; Turqueti, M.D.A.; Rossa, A.J.; Dezuo, T.J.M.; Barra, W. Robust Linear Parameter Varying Scalar Control Applied in High Performance Induction Motor Drives. *IEEE Trans. Ind. Electron.* **2020**, *68*, 10558–10568. [CrossRef]
21. Novak, H.; Lesic, V.; Vasak, M. Energy-Efficient Model Predictive Train Traction Control with Incorporated Traction System Efficiency. *IEEE Trans. Intell. Transp. Syst.* **2021**, 1–12. Available online: https://ieeexplore.ieee.org/document/9325928 (accessed on 22 December 2021). [CrossRef]
22. Jumaev, O.A.; Sayfulin, R.R.; Samadov, A.R.; Arziyev, E.I.; Jumaboyev, E.O. Digital control systems for asynchronous electrical drives with vector control principle. *IOP Conf. Ser. Mater. Sci. Eng.* **2020**, *862*, 032054. [CrossRef]
23. Botirov, T.V.; Latipov, S.B.; Buranov, B.M. About one synthesis method for adaptive control systems with reference models. *J. Phys. Conf. Ser.* **2020**, *1515*, 022078. [CrossRef]
24. Lee, J.-K.; Kim, J.-W.; Park, B.-G. Fast Anti-Slip Traction Control for Electric Vehicles Based on Direct Torque Control with Load Torque Observer of Traction Motor. In Proceedings of the 2021 IEEE Transportation Electrification Conference & Expo (ITEC), Chicago, IL, USA, 21–25 June 2021; pp. 321–326. [CrossRef]
25. Aissa, B.; Hamza, T.; Yacine, G.; Mohamed, N. Impact of sensorless neural direct torque control in a fuel cell traction system. *Int. J. Electr. Comput. Eng. (IJECE)* **2021**, *11*, 2725–2732. [CrossRef]
26. Karlovsky, P.; Lettl, J. Induction Motor Drive Direct Torque Control and Predictive Torque Control Comparison Based on Switching Pattern Analysis. *Energies* **2018**, *11*, 1793. [CrossRef]
27. Kumar, Y.S.; Poddar, G. Medium-Voltage Vector Control Induction Motor Drive at Zero Frequency Using Modular Multilevel Converter. *IEEE Trans. Ind. Electron.* **2017**, *65*, 125–132. [CrossRef]
28. Hassan, M.M.; Shaikh, M.S.; Jadoon, H.U.K.; Atif, M.R.; Sardar, M.U. Dynamic Modeling and Vector Control of AC Induction Traction Motor in China Railway. *Sukkur IBA J. Emerg. Technol.* **2020**, *3*, 115–125. [CrossRef]
29. Wang, H.; Liu, Y.; Ge, X. Sliding-mode observer-based speed-sensorless vector control of linear induction motor with a parallel secondary resistance online identification. *IET Electr. Power Appl.* **2018**, *12*, 1215–1224. [CrossRef]
30. Ćwil, M.; Bartnik, W.; Jarzębowski, S. Railway Vehicle Energy Efficiency as a Key Factor in Creating Sustainable Transportation Systems. *Energies* **2021**, *14*, 5211. [CrossRef]
31. Nurali, P.; Mirzaev, U. Ways to Improve the Energy Efficiency of an Electric Drive with Asynchronous Mo-tors. *Int. J. Eng. Inf. Syst. (IJEAIS)* **2021**, *5*, 230–233.
32. Pleshivtseva, Y.E.; Rapoport, E.Y. Parametric Optimization of Systems with Distributed Parameters in Problems with Mixed Constraints on the Final States of the Object of Control. *J. Comput. Syst. Sci. Int.* **2018**, *57*, 723–737. [CrossRef]
33. Pleshivtseva, Y.E.; Rapoport, E.Y. Optimal Energy-Efficient Programmed Control of Distributed Parameter Systems. *J. Comput. Syst. Sci. Int.* **2020**, *59*, 518–532. [CrossRef]
34. Rapoport, E.Y. Method for Parametric Optimization in Problems of the Multichannel Control of Systems with Distributed Parameters. *J. Comput. Syst. Sci. Int.* **2019**, *58*, 545–559. [CrossRef]
35. Razghonov, S.; Kuznetsov, V.; Zvonarova, O.; Chernikov, D. Track circuits adjusting calculation method under current influence traction interference and electromagnetic compatibility. *IOP Conf. Ser. Mater. Sci. Eng.* **2020**, *985*, 012017. [CrossRef]
36. Çelik, E. Incorporation of stochastic fractal search algorithm into efficient design of PID controller for an automatic voltage regulator system. *Neural Comput. Appl.* **2018**, *30*, 1991–2002. [CrossRef]

37. Weerakkody, S.; Liu, X.; Sinopoli, B. Robust structural analysis and design of distributed control systems to prevent zero dynamics attacks. In Proceedings of the 2017 IEEE 56th Annual Conference on Decision and Control (CDC), Melbourne, Australia, 12–15 December 2017; pp. 1356–1361. [CrossRef]
38. Kiumarsi, B.; Vamvoudakis, K.G.; Modares, H.; Lewis, F.L. Optimal and Autonomous Control Using Reinforcement Learning: A Survey. *IEEE Trans. Neural Netw. Learn. Syst.* **2018**, *29*, 2042–2062. [CrossRef] [PubMed]
39. Luo, B.; Yang, Y.; Liu, D.; Wu, H.-N. Event-Triggered Optimal Control with Performance Guarantees Using Adaptive Dynamic Programming. *IEEE Trans. Neural Netw. Learn. Syst.* **2020**, *31*, 76–88. [CrossRef]
40. Possieri, C.; Sassano, M. Deterministic Optimality of the Steady-State Behavior of the Kalman–Bucy Filter. *IEEE Control Syst. Lett.* **2019**, *3*, 793–798. [CrossRef]
41. Feliu-Batlle, V.; Feliu-Talegón, D.; San-Millan, A.; Rivas-Pérez, R. Wiener-Hopf optimal control of a hydraulic canal prototype with fractional order dynamics. *ISA Trans.* **2018**, *82*, 130–144. [CrossRef]
42. Zhao, G.; Qian, X.; Yoon, B.-J.; Alexander, F.J.; Dougherty, E.R. Model-Based Robust Filtering and Experimental Design for Stochastic Differential Equation Systems. *IEEE Trans. Signal Process.* **2020**, *68*, 3849–3859. [CrossRef]
43. Goolak, S.; Liubarskyi, B.; Sapronova, S.; Tkachenko, V.; Riabov, I.; Glebova, M. Improving a model of the induction traction motor operation involving non-symmetric stator windings. *East. Eur. J. Enterp. Technol.* **2021**, *4*, 45–58. [CrossRef]
44. Goolak, S.; Tkachenko, V.; Šťastniak, P.; Sapronova, S.; Liubarskyi, B. Analysis of Control Methods for the Traction Drive of an Alternating Current Electric Locomotive. *Symmetry* **2022**, *14*, 150. [CrossRef]
45. Yousefi-Talouki, A.; Pescetto, P.; Pellegrino, G.-M.L.; Boldea, I. Combined Active Flux and High-Frequency Injection Methods for Sensorless Direct-Flux Vector Control of Synchronous Reluctance Machines. *IEEE Trans. Power Electron.* **2018**, *33*, 2447–2457. [CrossRef]
46. Al-Gabalawy, M.; Hosny, N.S.; Dawson, J.A.; Omar, A.I. State of charge estimation of a Li-ion battery based on extended Kalman filtering and sensor bias. *Int. J. Energy Res.* **2021**, *45*, 6708–6726. [CrossRef]
47. Goolak, S.; Liubarskyi, B.; Sapronova, S.; Tkachenko, V.; Riabov, I. Refined Model of Asynchronous Traction Electric Motor of Electric Locomotive. In Proceedings of the 25th International Scientific Conference "Transport Means", Online, 6–8 October 2021; pp. 455–460.
48. Valluri, S.R.; Dergachev, V.; Zhang, X.; Chishtie, F.A. Fourier transform of the continuous gravitational wave signal. *Phys. Rev. D* **2021**, *104*, 024065. [CrossRef]
49. Han, X.; Xue, L.; Shao, F.; Xu, Y. A Power Spectrum Maps Estimation Algorithm Based on Generative Adversarial Networks for Underlay Cognitive Radio Networks. *Sensors* **2020**, *20*, 311. [CrossRef] [PubMed]